Cement and Concrete Research 42 (2012) 577–582

Contents lists available at SciVerse ScienceDirect

Cement and Concrete Research

journal homepage: http://ees.elsevier.com/CEMCON/default.asp

Hydration kinetics of cements by Time-Domain Nuclear Magnetic Resonance: Application to Portland-cement-derived endodontic pastes

William Bortolotti [a,*], Paola Fantazzini [b], Romano Mongiorgi [c], Salvatore Sauro [d,e], Silvano Zanna [c]

[a] Department DICAM, University of Bologna, Via Terracini 28, 40131, Bologna, Italy
[b] Department of Physics, University of Bologna, Viale Berti Pichat 6/2, 40127, Bologna, Italy
[c] Centre of Biomineralogy, Crystallography and Biomaterials, Department of Earth and Geoenvironmental Sciences, University of Bologna, Piazza di Porta S. Donato, 40127, Bologna, Italy
[d] Department of Dental Biomaterials Science Kings College, London Dental Institute at Guy's, King's College and St Thomas' Hospitals, Floor 17 Guy's Tower, Guys Hospital, London Bridge, London SE1 9RT, UK
[e] Dental Materials, School of Dentistry, University of Granada, Colegio Máximo, Campus de Cartuja, Granada, Spain

ARTICLE INFO

Article history:
Received 9 July 2011
Accepted 20 December 2011

Keywords:
NMR
Kinetics
Calcium–silicate–hydrate
Hydration products
Endodontic cements

ABSTRACT

Time-Domain Nuclear Magnetic Resonance (TD-NMR) of ^{1}H nuclei is used to monitor the maturation up to 30 days of three different endodontic cement pastes. The "Solid–liquid" separation of the NMR signals and quasi-continuous distributions of relaxation times allow one to follow the formation of chemical compounds and the build-up of the nano- and subnano-structured C–S–H gel. ^{1}H populations, distinguished by their different mobilities, can be identified and assigned to water confined within the pores of the C–S–H gel, to crystallization water and Portlandite, and to hydroxyl groups. Changes of the TD-NMR parameters during hydration are in agreement with the expected effects of the different additives, which, as it is known, can substantially modify the rate of reactions and the properties of cementitious pastes. Endodontic cements are suitable systems to check the ability of this non-destructive technique to give insight into the complex hydration process of real cement pastes.

1. Introduction

An ideal endodontic cement should have both biocompatibility/osteoconductive characteristics and good workability properties in order to be applied easily in the deep cavities subsequent to the removal of infected and degenerated tissue, and in zones of mineral-depleted tissue. Portland-type cements are widely used in dentistry and their clinical use is destined to increase due to the evolution of conservative therapy, the long term predictability of endodontic therapy, and the many patients affected by endodontic pathology, especially among the elderly [1]. These cements have been extensively studied and modified after the commercialization, in 1993, of the Mineral Trioxide Aggregate (MTA) [2–6]. They are mainly composed by a mixture of hydrophilic particles such as Tricalcium Silicate ($3CaO \cdot SiO_2$), Dicalcium Silicate ($2CaO \cdot SiO_2$), Tricalcium Aluminate ($3CaO \cdot Al_2O_3$) which react in presence of moisture. Several additives are employed within the composition of these cements in order to improve specific properties such as hydration kinetics, microstructure and setting properties.

A complex sequence of chemical–physical processes occur during the hydration of the powder which leads to the formation of Calcium Hydroxide ($Ca(OH)_2$, Portlandite) and a quasi-amorphous, poorly crystalline, Calcium Silicate Hydrate, called C–S–H gel made of calcium silicate particles with a layered structure.

These processes have been studied by different techniques. Small–angle neutron and X-ray scattering (SANS and SAXS) are able to measure structure properties over a scale ranging from nanometers to micrometers, but not at the internal sub-nanometers level of the particles [7]. Neutron and X-ray diffraction methods measure the Portlandite formation at the micrometer scale [8]. Quasi-elastic neutron scattering (QENS) can monitor the state of water, to distinguish free and bound water within cement and quantify their changes during the hydration process [8,9].

Allen et al. [7] gave a picture of the nanoscale C–S–H gel, represented in the form of nanometer scale particles, made of calcium silicate sheets containing OH^- groups, separated by inter-layer spaces with physically bound water. A thin layer of water is adsorbed on the surfaces of the particles and liquid water fills the nanopores between the particles.

In a recent computer simulation, the C–S–H is considered to be made of rather irregular sheets, with water adsorbed in the inter-layer regions (spacings a little over 1 nm) and in the distorted intra-layer regions around the silica monomers [10].

A major summary of up-to-date composition and crystal structure for the most important crystalline calcium (alumino) silicate hydrates is given in [11], but notwithstanding great progress in the understanding

* Corresponding author. Tel.: +39 0512090236; fax: +39 0512090457.
E-mail address: villiam.bortolotti@unibo.it (V. Bortolotti).

0008-8846/$ – see front matter © 2011 Elsevier Ltd. All rights reserved.
doi:10.1016/j.cemconres.2011.12.006

of mechanisms of cement hydration and microstructure development [12,13] research is still needed for a better understanding of the chemistry and physics of hydration kinetics [12].

Also nuclear magnetic resonance (NMR) techniques [14] have been applied to study the formation and nanostructure of the cements, including diffusometry [15], imaging [16,17] and relaxometry (NMR in the time domain, TD-NMR) [18–29]. It is long known that the relaxation rates R_1 and R_2 (reciprocals of the relaxation times of the longitudinal (T_1) and transverse (T_2) components of the ^{1}H nuclear magnetization) of a pore fully saturated with water, under the condition of fast diffusion, if the relaxation rates of the bulk (not confined) water are negligible, are proportional to the surface-to-volume ratio (S/V) of the pore ($1/T_{1,2} = \rho_{1,2}S/V$): the larger the pore, the longer the relaxation time of water ^{1}H nuclei. The constants of proportionality $\rho_{1,2}$ are called surface relaxivities (longitudinal and transverse, respectively) [30]. In Ref. [18] the spaces of the gel pores are estimated to range from 10 nm down to less than 0.5 nm, and in Ref. [19] the thickness of tightly bound gel water layers between the sheets is given as about 1–2 nm. Two-Dimensional Inverse Laplace Transform (2D-ILT) T_1–T_2 and T_2–T_2 experiments showed a distribution of pore sizes [20–24,26], and an exchange between two different structures in the gel was suggested. One pore size was evaluated after four days of curing to be of the order of 1 nm, and another in the range from about 10 up to about 25 nm (2.4 nm and 16 nm in Ref. [26]). An alternate explanation of the NMR data could be the exchange between two classes of pores of comparable sizes, but different surface relaxivity. New experiments have shown that this alternate explanation almost certainly does not apply [28].

In a recent study [29] the well known [18,27] existence of a population of very low mobility protons has been investigated by TD-NMR. ^{1}H nuclei of water in capillaries (larger pores) and in C–S–H gel can be resolved from those in solid phases, such as hydroxyl groups of Portlandite and crystal water, thanks to the effect on T_2 of molecular mobility. The nuclei with lower-mobility, hereinafter called “solid-like”, give signal decays of quasi-Gaussian form with T_2 on the order of 10 μs, orders of magnitude shorter than T_2 for exponential decay of the higher-mobility nuclei, hereinafter “liquid-like”. Only a few NMR studies of cements in different conditions have taken advantage of this opportunity [18,27,29]. In Ref. [29], where relaxation analysis was performed on progressively dried white cement paste, the gel was considered as composed of tetrahedral silica layers interspersed with layers of water and calcium ions in a sheet-like structure (intra-C–S–H sheet water), randomly stacked with water in inter-C–S–H-gel pore space. By the ratio of the solid echo to Free Induction Decay (FID) signal amplitudes the authors could estimate the relative specific area and the width of intra-C–S–H sheets and inter-C–S–H gel pores, found in their experimental conditions to be 1.5 nm and 4.1 nm thick, respectively.

The maturation of the commercial endodontic cement (MTA) has been studied in Ref. [27]. T_1 and T_2 quasi-continuous distributions analysis was performed during hydration from 1 h to 30 days. The separation of solid-like and liquid-like components has been made on the FID signals, giving a 2D analysis on the physical basis of different ^{1}H mobility. After about a day two clearly solid-like components appear, while from a day to a few days at least two liquid-like populations can be identified, which progressively merge, giving a single T_1 or T_2 peak. The growth of the solid-like population at the cost of the liquid-like was shown, along with the rapid changes of the T_1 and T_2 distributions of all components reflecting the formation and evolution of the reaction products (C–S–H gel and Portlandite) and of the C–S–H micro-nano-porous structure. At 30 days of hydration, a very short T_1 and T_2 liquid-like component ($T_1 \cong 200$ μs and $T_2 \cong 50$ μs) was assigned to C–S–H intra-layer water (thickness of the order of fractions of a nanometer) and the remaining liquid-like signal to interlayer water (thickness of the order of 1 nm).

Recently, two new varieties of Portland-type endodontic cements [31–34] have been commercialized with specific additive compounds to make the hydration process faster and to improve the workability and the mechanical, chemical, physical and biological properties [33]. Preliminary results have shown [27] that TD-NMR parameters can distinguish the different hydration kinetics of the different cement pastes.

In this study the extensive and detailed analysis of relaxation time distributions performed on MTA has been repeated and performed on these two new endodontic cement pastes, with particular attention to the evolution of the T_1 distribution of the solid-like component, separated from the liquid-like one. The goal is to see how much these TD-NMR methods are able to distinguish the evolution of the different pastes, not only in order to give an efficient tool to study endodontic cements, but also to give some more insight on the formation kinetics of the chemical products and on the nanostructure formation of the C–S–H gel in real cementitious materials.

2. Materials and methods

2.1. Sample preparation

Three endodontic cements, obtained starting from Portland Cement were studied. MTA (ProRoot MTA, Dentsply Tulsa Dental Products, Tulsa, OK), is a Portland Cement with bismuth oxide added to increase its radio-opacity, assumed as a reference (hereinafter R). TECHBIOSEALER *Standard* (hereinafter S) (ISASAN s.r.l., Como, Italy) is a White Portland Cement (WPC) with added calcium chloride (5% by weight), which increases the initial rate of setting. TECHBIOSEALER *Fluoridated* (hereinafter F) (ISASAN s.r.l, Como, Italy), is a WPC with added calcium sulfate (1% by weight), to control the setting and to slow down the hydration process, and sodium fluoride (1% by weight) which provides F-ions to the structure of the enamel of the tooth and gives the cement paste longer working time. The last two cements have phyllosilicate added (montmorillonite 1% in weight), a filler which makes water molecules available during setting, and 15% by weight of bismuth oxide. The initial particle sizes are less coarse for samples F and S than for regular WPC, as the WPC grains were ground small.

All samples were pastes prepared by adding 250 mg of water to 500 mg of powder and mixed at the bottom of a 10 mm external diameter glass NMR tube. This procedure was chosen to mimic the odontoiatric preparation. The TD-NMR measurements were performed from 1 h to 30 days after water addition. In total, a dozen of samples were analyzed to check the reproducibility of the observed behaviors of the cement pastes.

2.2. SEM analysis

For the morphological and elemental analysis a Scanning Electron Microscope equipped with an energy-dispersive X-ray spectrometer was used (SEM Philips 515 / EDX-EDAX Dx 4) with 20 kV accelerating voltage, that excited a volume of about 16 μm^3. Four samples from each cement paste were examined under SEM.

SEM images taken at 30 days for one sample for each kind of cement paste (S, F and R), along with their elemental compositions, are shown in Fig. 1.

2.3. Time-Domain Nuclear Magnetic Resonance

A relaxometer based on a JEOL electromagnet working at 0.47 T, corresponding to a Larmor frequency of about 20 MHz for ^{1}H nuclei, equipped with a Spinmaster console (Stelar, Mede, PV, Italy), was used. Longitudinal relaxation curves for T_1 measurements were acquired at 25 °C by Inversion-Recovery (IR) pulse sequences ($\pi_x - t - (\pi/2)_x -$ FID acquisition) [14]. CPMG sequences with 40 μs echo time were used for

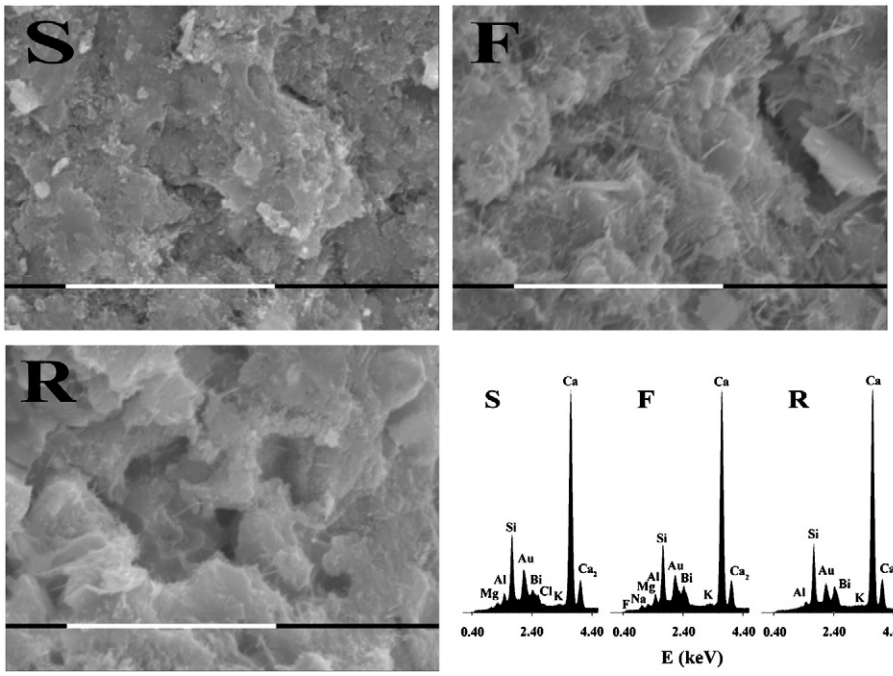

Fig. 1. SEM and EDX analyses on the fracture surfaces of the three cement pastes after 30 days of hydration. The samples are: S (White Portland Cement with added $CaCl_2$), F (White Portland Cement with added NaF), R (MTA, White Portland Cement). The marker is 10 μm. The morphology is different even at this scale. Each image is representative of the whole sample and of the paste. The x-axis of the EDX spectra is the energy of the X-ray in keV; the y-axis is the intensity of the X-ray signal (areas proportional to the counts). The second peak of Calcium refers to k_β transitions.

T_2 relaxation time measurements. Relaxation decay data were inverted to give relaxation time distributions by the algorithm UPEN [35,36], implemented in UpenWin software [37]. At least two ^{1}H nuclei populations were visible on the FIDs of IR data sets, and the two were separated by fitting each FID to the sum of a quasi-Gaussian and an exponential. The quasi-Gaussian corresponds to low-mobility ^{1}H, the solid-like population, and the exponential to higher-mobility ^{1}H, the liquid-like population. The ratio of the two extrapolated signals gives the solid-like -to- liquid-like ^{1}H ratio α. The relaxation time of the liquid-like component measured on the FID will be called in the following T_{2FID}, with the corresponding rate, $R_{2FID} = 1/T_{2FID}$. For more experimental details see [27,38].

3. Results

The general characteristics of the changes over hydration time of NMR signals observed in Ref. [27] are present in all the samples examined in this study. Details of these characteristics differentiate the different endodontic cement pastes, as confirmed by checking different samples for each paste. The signal amplitude of the solid-like population increases at the expense of the liquid-like during ageing, so that a continuous increase of α (see Fig. 2a) is seen, with a different behavior for the three pastes. F shows the same initial behavior as R, with α about constant for the first few hours and with a steep increase at about 10 h. S shows a larger solid-like component already in the very first hours, with a α ratio that starts to increase rapidly right from the beginning of hydration. After 30 days, α is in the range of 20–40% depending on the sample. Fig. 2b shows the evolution of the FID decay rates R_{2FID} for the three samples of Fig. 2a. This parameter shows different kinetics in the course of the first 50 h, with a faster initial increase for sample S. Because of the large liquid-like signal amplitude, R_{2FID} is a robust parameter useful to monitor the changes of the environment of the liquid-like ^{1}H nuclei. It should be noted that the FID decay of the liquid-like population is not a single-exponential.

A detailed analysis of the evolution is obtained by the behavior over time of the quasi-continuous T_1 and T_2 distributions. Figs. 3, 4 and 5 show the distributions at selected hydration times for samples S, F and R of cement pastes. The same arbitrary units are used in all parts of Figs. 3–5, but it should be noted that, because of the Inversion-Recovery measurement sequence used, the signal for T_1 is

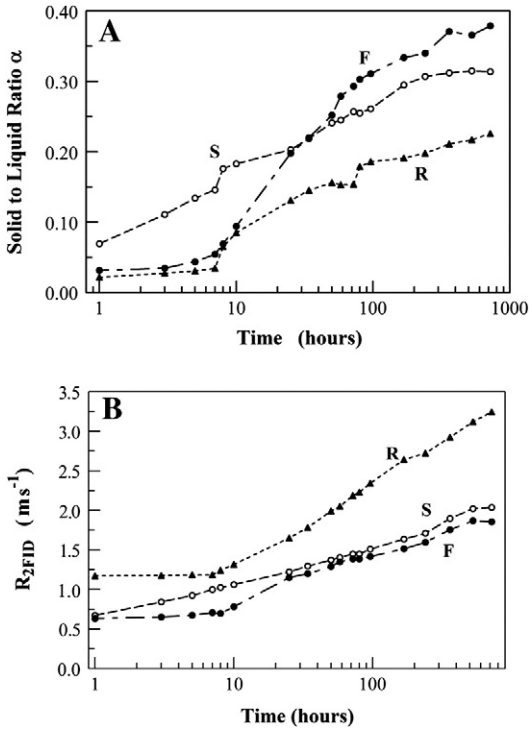

Fig. 2. Ratio of solid-like to liquid-like signals α (a) and liquid-like FID decay rate R_{2FID} (b) as functions of hydration time for the three pastes. R_{2FID} in the three pastes increases as the pore space structure of the C–S–H gel forms. The parameters α and R_{2FID} both increase initially more rapidly for sample S than for F and R. The different behaviors of F and S reflect the different uses for which these cement pastes have been planned.

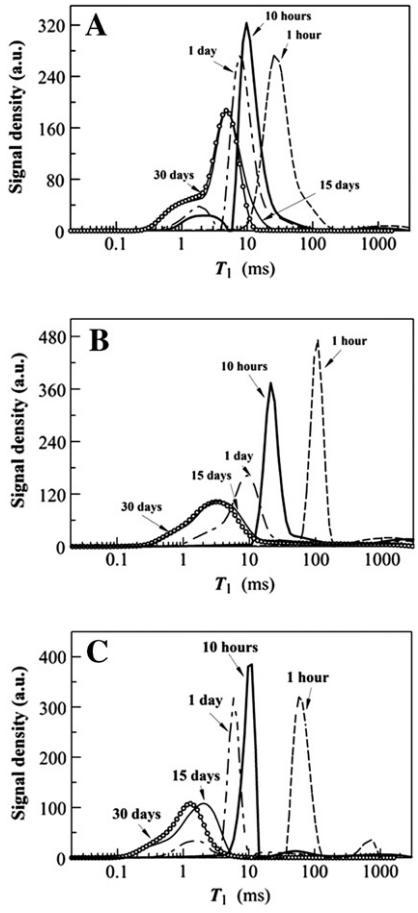

Fig. 3. A selection of quasi-continuous T_1 relaxation time distributions as functions of ageing time for the higher mobility component of the pastes: S (a), F (b) and R (c). In all cases, the peaks shift to shorter relaxation times with ageing. For S, a second (incompletely resolved) peak is recognizable even after 30 days. For F only one peak is visible from the beginning of the process up to 30 days, although a slight tail is seen toward short times.

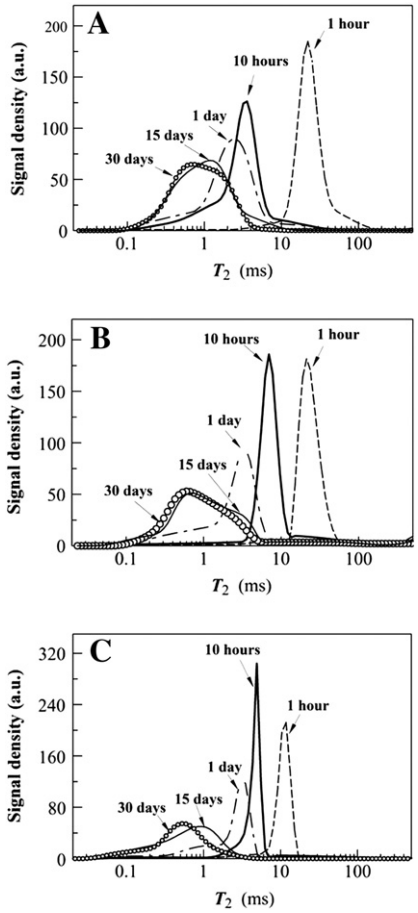

Fig. 4. A selection of quasi-continuous T_2 relaxation time distributions of the higher mobility component as a function of ageing time for the samples of Fig. 3. As for the distributions in Fig. 3, the distributions are shifted at 30 days to very short relaxation times, consistent with the model of water molecules absorbed in intra-layer (half nanometer or less) and inter-layer (in the range of a nanometer) spaces of the C–S–H gel.

about double than for T_2. Figs. 3 and 4 are for the liquid-like, Fig. 5 for the solid-like. The T_1 distribution of the liquid-like (Fig. 3) shows a small liquid-like signal at times longer than 100 ms, which is due to water in large pores (capillary pores). The comparison at short ageing or hydration times shows different behaviors. At 1 h, samples R and F show sharp T_1 peaks centered at about 60 ms and 100 ms, respectively. For sample S the peak is broader and ranges from 10 to about 100 ms. For all samples this peak shifts to shorter times and shows reduced area with ageing, and the timing and shapes of the changes are different for the different cement pastes. At 1 day, as observed in Ref. [27], MTA (R) shows two resolved peaks, in the range 0.4–10 ms, that then merge into only one peak, which shifts to shorter and shorter times. After 30 days the peak covers the range from 0.1 ms to a few ms. The distribution for paste S shows two early peaks; the peak at shorter times is already visible at less than 10 h. The two peaks never fully merge into only one: at 30 days the two peaks are still evident, although not fully resolved, in the range 0.3–10 ms. Cement paste F is characterized by a single liquid-like peak, which decreases in amplitude, broadening and shifting to shorter relaxation times. At 30 days the peak covers the range between 0.2 and 10 ms. In summary, at 30 days the distributions for S, F and R show substantial differences: F shows only one peak, S shows two unresolved peaks, R shows a peak at shorter times than F and at about the time of the shorter-time unresolved peak of S.

The shifts to shorter relaxation times with ageing are shown also by T_2 distributions (Fig. 4), with less ability to characterize the different cement pastes. It is worth noting that at longer hydration times T_2 distributions show a tail down to 100 μs for S and F, and still less for R, that is, shorter than the corresponding T_{2FID} values, 300–700 μs (see Fig. 2b for $R_{2FID} = 1/T_{2FID}$). This signal is due to short-T_2 nuclei, with T_2 values intermediate between the lowest-mobility nuclei (T_2 on the order of 10 μs), and the nuclei assigned to the liquid-like component with much longer T_{2FID}. These nuclei should correspond to the nuclei with the shortest T_1 in Fig. 3; otherwise there would be nuclei with T_1 less than T_2, not physically acceptable. That means that a liquid-like component with very short T_2 and T_1 has been partly assigned to the liquid-like and partly to the solid-like in our solid–liquid FID-separation.

Fig. 5 shows a selection of T_1 distributions of the solid-like population for S (5a), F (5b) and R (5c). At 1 h only a very wide low peak from 0.2 to 1000 ms is observed in S and from 0.2 to less than 10 ms in F and R. At 10 h the signals are higher, the distributions are more reliable, and they start to suggest the presence of more than one group of solid-like spins. At 1 day one can observe the growth of the signal in the 0.1–10 ms range and also a peak at hundreds of ms for all the samples. At longer hydration times all samples have the peak at longer T_1, and the peaks at lower T_1 are quite different for the three cements.

4. Discussion

It is difficult to compare NMR data from the literature because they refer to different preparations and often to very different

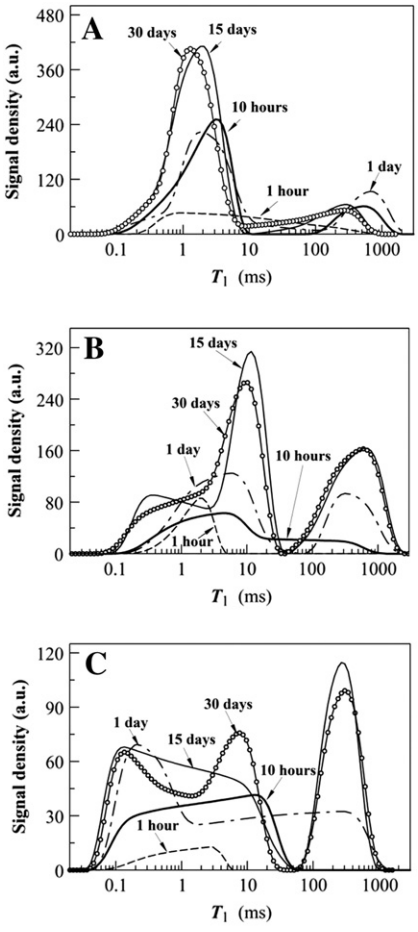

Fig. 5. A selection of T_1 relaxation time distributions as functions of ageing time for the lower mobility components of the samples in Figs. 3 and 4. The T_1 peak at longer times can be assigned mainly to ^{1}H of crystal water and $Ca(OH)_2$ (Portlandite) and the peak with intermediate T_1 to ^{1}H nuclei of Ca–OH and Si–OH groups. The shoulder or extension to shorter times may be part of a population with very short T_1 and T_2, partly attributed to the liquid-like and partly to the solid-like in our solid–liquid separation of the FIDs.

hydration times. The results of this paper highlights how the choice of the hydration time is extremely important for consistent comparisons since the TD-NMR parameters change over time significantly and in different ways for different preparations.

The increase of the solid-like component at the cost of the liquid-like, with the corresponding increase of the α parameter (Fig. 2), is due to the chemical reactions leading to the progressive production of Portlandite and the formation of C–S–H gel, at the cost of the water molecules initially added to the cement powder. The kinetics of the formation of the solid-like population shows that cement S has the most rapid initial evolution, with α larger than 5% already at 1 h and reaching a value larger than 15% at 7 h, while cements F and S are still at the initial low value. F behaves as R in the first few hours, with slower initial changes, and then shows a strong acceleration later, in the period between 10 h and 2 days. It is known that $CaCl_2$ is an accelerator [13,39], and an acceleration is expected in S [40,41]. Our data show clearly the effect of this additive, with the fast growth of the α value in sample S in the first 10 h. The lower acceleration of cement F during the first period of ageing might be related to the added calcium sulfate.

Moreover, the pore space structure changes in different ways for the different cement pastes, this is shown in one way by the behavior of the parameter R_{2FID} (Fig. 2b), related to the changes of the sizes of the pores confining liquid water (the larger the rates, the smaller the pore-sizes) and in a more detailed way by the T_1 and T_2 distributions of the liquid-like population in Figs. 3 and 4. The evolution of the T_1 and T_2 distributions can be associated with C–S–H gel build-up, thanks to the dependence of relaxation times on the surface-to-volume ratios of the pores. The changes and the shifts of the distributions in Fig. 3 reflect the gradual formation and reduction in pore sizes in the C–S–H gel. The progressive buildup of the pore structure of the gel, with higher and higher surface-to-volume ratios, leads to shorter and shorter relaxation times as the process of hardening proceeds, in different ways in the different cements, reflecting the different kinetics and the different structure at 30 days of the three cements, with cement R exhibiting shorter liquid-like relaxation times than S and F.

Our data are in accordance with the diagram of C–S–H particles given in [7]. The liquid-like with longer T_1 is from water in larger spaces. The tail of the T_1 distributions at shorter times can be assigned at the sub-nanometer scale. By assuming [30] a surface relaxivity on the order of 1 μm/s for T_1, one can achieve the estimation of characteristic pore sizes. At the end of the 30 days period, the tail at very short times (0.2–0.3 ms for S and F, and 0.1 ms for R) should correspond to spacings of a half nanometer or less, that may correspond to intra-layer spaces of the gel. The relaxation times at about 1 ms and more should correspond to inter-layer or inter-grain spaces on the order of nanometers. This is consistent with the results of the computer simulation described in [10].

After 30 days, the T_1 distribution of the liquid-like of S in Fig. 3 suggests two unresolved components at short times, with a larger amount of water in the nanometer spaces for S than for F and R. This suggests that the hydration process of S is probably not yet complete. At this stage the $CaCl_2$ additive, which initially accelerates the formation of the solid-like component, slows down the hydration kinetics later. The results are in agreement with the expected behavior of cement pastes S and F, planned for different uses. F paste is less viscous immediately after preparation, so it can be easily inserted in the endodontial canal and then sealing it [34]. S paste hardens more quickly, so it is more suitable for retrograde endodontic practice [31,34].

The T_1 distributions for the solid-like ^{1}H components of the three cement pastes (Fig. 5) show gradual formation over time of two peaks and a shoulder at shorter times. This is consistent with the reported results obtained using also high resolution Magic Angle Spinning to suppress the effect of dipole–dipole interactions [21,26]. In these works five populations of ^{1}H nuclei have been found at three months of hydration. In addition to the ^{1}H of water, a population of ^{1}H with T_1 of 1 ms was assigned to Si–OH group, probably located within the intralayers of C–S–H; the T_1 on the order of 10^3 ms was assigned mainly to Portlandite; the peaks with intermediate T_1 were assigned to ^{1}H mobile species of Ca–OH and Si–OH groups and water, in fast exchange with the bulk in different classes of C–S–H pores [21,26]. In Fig. 5, the T_1 peak at longer times (100–1000 ms) can be assigned mainly to ^{1}H of the $Ca(OH)_2$ group of crystals of Portlandite; the signal with intermediate and lower T_1 values can be assigned to ^{1}H species of Ca–OH and Si–OH groups, the shoulder, or extension to about 0.1 ms, may be part of the liquid-like population mentioned in the Results with very short T_1 and T_2, partly attributed to the liquid-like and partly to the solid-like in our solid–liquid separation of the FIDs.

A comparison can be made of our results with the QENS [8,9,12]. By using the definition given in Ref. [9], the Bound Water Index (BWI) is given by the ratio of the bound to total water, defined as:

$$BWI = (A + B)/(A + B + C),$$

where, A is associated with the chemically bound hydrogen atoms, B is the constrained water (adsorbed onto pore surfaces, and contained within the nanoscale gel pores of C–S–H), and C is free (liquid) water.

In Ref. [9] for a tricalcium silicate paste, BWI increased from much less than 5% to about 55% during the first day of hydration (their Fig. 1). By considering the 24 h data in our Figs. 3 and 5, and assuming

as bound water the sum of the amount of signals in the peaks below about 3 ms in Fig. 3 (constrained water) plus the total solid-like signal of Fig. 5 (crystal water, ^{1}H nuclei in Portlandite, and in Ca–OH and Si–OH groups), and as free water the signal in the peaks at about 10 ms in Fig. 3, one gets for BWI 30.2%, 30.7% and 25.4% for S, F and R respectively. The lower values can be justified by the larger water/cement ratio used in our sample preparation, and with the addition to cements S and F of phyllosilicates, a filler which makes water molecules available during setting.

5. Conclusion

Notwithstanding continuous progress in the understanding of the morphology of the C–S–H gel, questions still are open that need a better knowledge of the water mass fraction and location [7]. TD-NMR analysis of ^{1}H nuclei can help in getting a deeper insight into the state of water, the sizes of the space where water is confined at the nanometer and sub-nanometer scales and the kinetics of the formation of the compounds containing ^{1}H nuclei. TD-NMR can monitor and quantify the kinetics of reaction products formation and nanostructure evolution, with the continuous changes of ^{1}H signals from liquid-like to solid-like, corresponding to the formation of crystallization water and of the OH groups in the calcium silicate layers and in Portlandite. Our data show, for the cements analyzed, different kinetics of the onset of the solid-like signal, as expected, and different structures of the gel at 30 days, and are in full agreement with the expected behavior of cement pastes S and F, that have different additives, planned for different endodontic uses.

Moreover, this kind of analysis, able to distinguish and quantify signals from low and higher mobility ^{1}H nuclei through the solid–liquid separation, and to follow their evolutions in terms of quantities and characteristics through the quasi-continuous distributions of relaxation times, can be used to compare real cement pastes in a non-destructive way not requiring radio-protection, in order to optimize their performances for different applications.

Acknowledgements

The authors thank R. J. S. Brown for useful discussions. This work was supported by the University of Bologna [Strategic project BIOENDO, ID number 487].

References

[1] I. Rotstein, R. Salehrabi, J.L. Forrest, Endodontic treatment outcome: survey of oral health care professionals, J. Endod. 32 (5) (2006) 399–403.
[2] M. Torabinejad, T.F. Watson, T.R. Pitt Ford, Sealing ability of a mineral trioxide aggregate when used as a root end filling material, J. Endod. 19 (1993) 591–595.
[3] E.T. Koh, M. Torabinejad, T.R. Pitt Ford, K. Brady, F. McDonald, Mineral trioxide aggregate stimulates a biological response in human osteoblasts, J. Biomed. Mater. Res. 37 (1997) 432–439.
[4] H.R. Abedi, J.I. Ingle, Mineral Trioxide Aggregate: a review of a new cement, J. Calif. Dent. Assoc. 23 (12) (1995) 36–39.
[5] M. Parirokh, M. Torabinejad, Mineral trioxide aggregate: a comprehensive literature review-Part III: clinical applications, drawbacks, and mechanism of action, J. Endod. 36 (3) (2010) 400–413.
[6] M. Parirokh, M. Torabinejad, Mineral trioxide aggregate: a comprehensive literature review-Part I: chemical, physical, and antibacterial properties, J. Endod. 36 (1) (2010) 16–27.
[7] A.J. Allen, J.J. Thomas, H.M. Jennings, Composition and density of nanoscale-calcium-silicate-hydrate in cement, Nat. Mater. 6 (2007) 311–316.
[8] A.J. Allen, J.J. Thomas, Analysis of C-S-H gel and cement paste by small-angle neutron scattering, Cement Concr. Res. 37 (2007) 319–324.
[9] J.J. Thomas, S.A. FitzGerald, D.A. Neumann, R.A. Livingston, State of water in hydrating tricalcium silicate and Portland cement pastes as measured by Quasi-Elastic Neutron Scattering, J. Am. Ceram. Soc. 84 (8) (2001) 1811–1816.
[10] R.J.-M. Pellenq, A. Kushima, R. Shahsavari, K.J. Van Villet, M.J. Buehler, S. Yip, F.-J. Ulm, A realistic molecular model of cement hydrates, Proc. Natl. Acad. Sci. U. S. A. 106 (2009) 16102–16107.
[11] I.G. Richardson, The calcium silicate hydrates, CCR 38 (2008) 137–158.
[12] J.W. Bullard, H.M. Jennings, R.A. Livingston, A. Nonat, G.W. Scherer, J.S. Schweitzer, K.L. Scrivener, J.J. Thomas, Mechanisms of cement hydration, Cement Conc. Res. 41 (12) (2011) 1208–1223.
[13] J.J. Thomas, J.J. Biernacki, S. Bishnoi, J.S. Dolado, G.W. Scherer, A. Luttge, Modeling and simulation of cement hydration kinetics and microstructure development, Cement Conc. Res. 41 (12) (2011) 1257–1278.
[14] R. Kimmich, NMR Tomography, Diffusometry, Relaxometry. Ed. Springer-Verlag, 1997, 530 pp.
[15] N. Nestle, P. Galvosas, J. Kärger, Liquid-phase self-diffusion in hydrating cement pastes – results from NMR studies and perspectives for further research, Cement Concr. Res. 37 (2007) 398–413 and references therein.
[16] P.J. Prado, B.J. Balcom, S.D. Beya, R.L. Armstrong, T.W. Bremner, P.E. Grattan-Bellew, Concrete/mortar water phase transition studied by single-point MRI methods, Magn. Reson. Imaging 16 (1998) 521–523.
[17] S.D. Beyea, B.J. Balcom, T.W. Bremner, P.J. Prado, A.R. Cross, R.L. Armstrong, P.E. Grattan-Bellew, The influence of shrinkage-cracking on the drying behaviour of White Portland cement using Single-Point Imaging (SPI), Solid State NMR 13 (1998) 93–100.
[18] J. Greener, H. Peemoeller, C. Choi, R. Holly, E.J. Reardon, C.M. Hansson, M.M. Pintar, Monitoring of hydration of white cement paste with proton NMR spin-spin relaxation, J. Am. Ceram. Soc. 83 (2000) 623–627.
[19] A. Leventis, D.A. Verganelakis, M.R. Halse, J.B. Webber, J.H. Strange, Capillary imbibition and pore characterization in cement pastes, Transport Porous Med. 39 (2000) 143–157.
[20] P.J. McDonald, J.-P. Korb, J. Mitchell, L. Monteilhet, Surface relaxation and chemical exchange in hydrating cement pastes: a two-dimensional NMR relaxation study, Phys. Rev. E 72 (2005) 011409–9.
[21] A. Plassais, M.-P. Pomiès, N. Lequeux, J.-P. Korb, D. Petit, F. Barberon, B. Bresson, Microstructure evolution of hydrated cement pastes, Phys. Rev. E 72 (2005) 041401–041408.
[22] L. Monteilhet, J.-P. Korb, J. Mitchell, P.J. McDonald, Observation of exchange of micropore water in cement pastes by two-dimensional T2-T2 nuclear magnetic resonance relaxometry, Phys. Rev. E 74 (2006) 061404–061409.
[23] J.-P. Korb, Microstructure and texture of cementitious porous materials, Magn. Reson. Imaging 25 (2007) 466–469.
[24] P.J. McDonald, J. Mitchell, M. Mulheron, L. Monteilhet, J.-P. Korb, Two-dimensional correlation relaxation studies of cement pastes, Magn. Reson. Imaging 25 (2007) 470–473.
[25] P.F. Faure, S. Rodts, Proton NMR relaxation as a probe for setting cement pastes, Magn. Reson. Imaging 26 (2008) 1183–1196.
[26] J.-P. Korb, NMR and nuclear spin relaxation of cement and concrete materials, Curr. Opin. Colloid Interface Sci. 14 (2009) 192–202.
[27] M. Gombia, V. Bortolotti, B. De Carlo, R. Mongiorgi, S. Zanna, P. Fantazzini, Nanopore structure buildup during endodontic cement hydration studied by time-domain nuclear magnetic resonance of lower and higher mobility ^{1}H, J. Phys. Chem. B 114 (2010) 1767–1774.
[28] A. Valori, V. Rodin, P.J. McDonald, On the interpretation of ^{1}H 2-dimensional NMR relaxation exchange spectra in cements: Is there exchange between pores with two characteristic sizes or Fe^+ concentrations? CCR 40 (2010) 1375–1377.
[29] P.J. McDonald, V. Rodin, A. Valori, Characterisation of intra- and inter-C-S-H gel pore water in white cement based on an analysis of NMR signal amplitudes as a function of water content, CCR 40 (2010) 1656–1663.
[30] G.C. Borgia, R.J.S. Brown, P. Fantazzini, Nuclear magnetic resonance relaxivity and surface-to-volume ratio in porous media with a wide distribution of pore sizes, J. Appl. Phys. 79 (1996) 3656–3664.
[31] M.G. Gandolfi, S. Sauro, F. Mannocci, S. Zanna, M. Capoferri, C. Prati, R. Mongiorgi, New tetrasilicate cement as retrograde filling material: an in vitro study on fluid penetration, J. Endod. 33 (2007) 1082–1085.
[32] M.G. Gandolfi, S. Pagani, F. Perut, G. Ciapetti, N. Baldini, R. Mongiorgi, C. Prati, Innovative silicate-based cements for endodontics: a study of osteoblast-like cell response, J. Biomed. Mater. Res. 86A (2008) 477–486.
[33] M.G. Gandolfi, F. Perut, G. Ciapetti, R. Mongiorgi, C. Prati, New Portland cement-based materials for endodontics mixed with articaine solution: a study of cellular response, J. Endod. 34 (2008) 39–44.
[34] R. Mongiorgi, M.G. Gandolfi, C. Prati, Composition for use in dentistry, Application PCT/EP2008/051583, Alma Mater Studiorum-Università di Bologna, 2008.
[35] G.C. Borgia, R.J.S. Brown, P. Fantazzini, Examples of marginal resolution of NMR relaxation peaks using UPEN and diagnostics, Magn. Reson. Imaging 19 (2001) 473–475.
[36] P. Fantazzini, R.J.S. Brown, Units in distributions of relaxation times, Concept Magn. Reson. 27A (2) (2005) 122–123.
[37] V. Bortolotti, R.J.S. Brown, P. Fantazzini, UpenWin: a software to invert multi-exponential decay data, , 2009 Distributed by University of Bologna: villiam.bortolotti@unibo.it.
[38] P. Fantazzini, V. Bortolotti, R.J.S. Brown, M. Camaiti, C. Garavaglia, R. Viola, G. Giavaresi, Two ^{1}H-NMR methods to measure internal porosity of bone trabeculae: by solid–liquid signal separation and by longitudinal relaxation, J. Appl. Phys. 95 (2004) 339–343.
[39] J.J. Thomas, A.J. Allen, H.M. Jennings, Hydration Kinetics and Microstructure Development of Normal and $CaCl_2$-Accelerated Tricalcium Silicate Pastes, J. Phys. Chem. C 113 (2009) 19836–19844.
[40] E.A. Bortoluzzi, N.J. Broon, C.M. Bramante, R.B. Garcia, I.G. de Moraes, N. Bernardineli, Sealing Ability of MTA and Radiopaque Portland Cement With or Without Calcium Chloride for Root-End Filling, J. Endod. 32 (9) (2006) 897–900.
[41] S.T. Hong, K.S. Bae, S.H. Baek, K.Y. Kum, W. Lee, Microleakage of accelerated mineral trioxide aggregate and Portland cement in an in vitro apexification model, J. Endod. 34 (1) (2008) 56–58.